The figure is organized by the depths of sensors, thus, there are six sub-figures at six different depths. In each sub-figure, there are two acceleration curves from distinct accelerometers at the same depth in two different arrays. According to Figure 2, the acceleration time histories in the sand layer shows a high consistency, indicating that the centrifuge model has a good quality with uniform sand deposit and consistent accelerometer depths within the sand deposit. The slight divergence of acceleration time histories in the two different arrays within the lead shot layer might be caused by the loose state of the lead shot, indicated by the smoothly decreased gap with depth with maximum divergence less than 10%, which is acceptable in analysis.

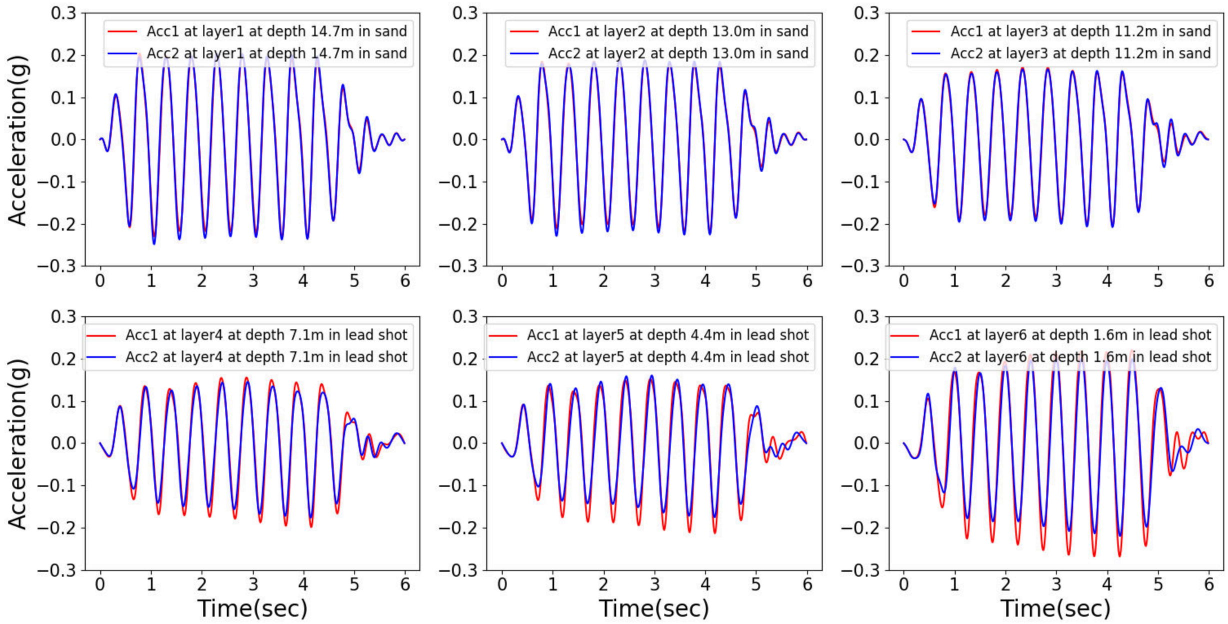

Figure 2. Acceleration time histories at the same depth from different arrays

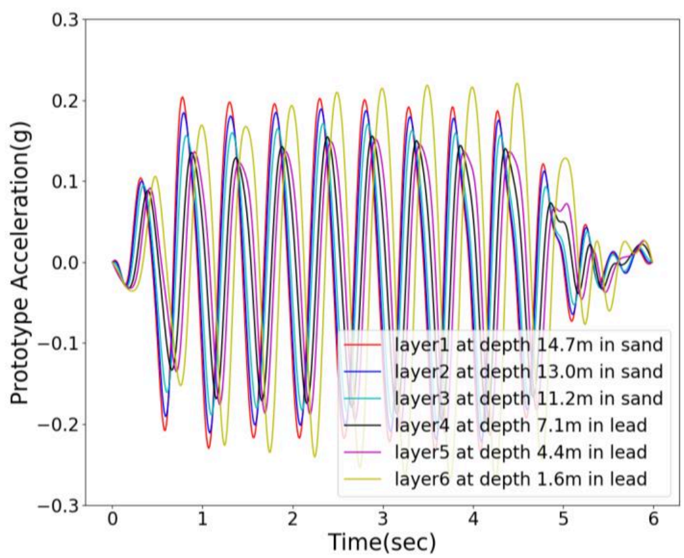

Figure 3. Acceleration time histories at different depths from the same array

The acceleration time histories inside the model at different depths are displayed in Figure 3, and the curves are from the same array with different depths. According to Figure 3, there is out of phase phenomena for acceleration curves at different depths, and the out of phase degree of the six curves at different depths was corresponding to the distance between the sensor location and the soil bottom, where the base acceleration happened. In other words, the longer the distance was, the later the seismic wave arrived. And the out of phase level in the lead shot was more apparent because there are increased distance gaps of accelerometers in the lead shot layer than that in the sand deposit. The acceleration amplitudes with depth are affected by the stiffness of material around the accelerometers.

Pore Pressure Build-up and Dissipation

Figure 4 shows the excess pore pressure build-up and dissipation with time at different depths in the same array. Based on Figure 4, the following phenomenon were observed: 1) the pore pressure transducers at the bottom three layers took around 3 cycles to complete all the excess pore pressure build-up. Also they arrived the maximum pore pressure buildup nearly at the same moment; 2) the pore pressure dissipation rates at different depths were very similar, showing the consistent viscosity of the viscous fluid used for saturation, and all the pore pressure dissipation also finished at the same moment; 3) the magnitude of excess pore pressure buildup decreased with depth, that is, the excess pore pressure buildup at the surface layer was the least, nearly close to none because the sand model has a free dissipation surface due to the dry lead shot layer on top of the sand model.

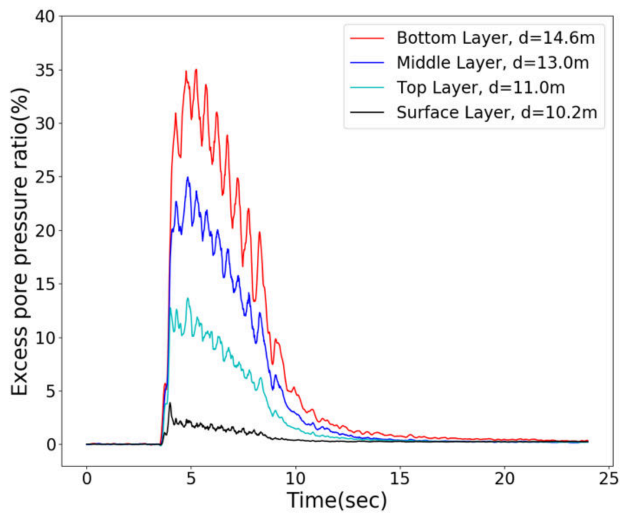

Figure 4. Excess pore pressure build-up at different depths during shake 2

Excess Pore Pressure Profile

The excess pore pressure profiles at four different times during excess pore buildup and dissipation are shown in Figure 5.

According to Figure 5, the excess pore pressure, Δu, at water level was always zero. Δu at all depths were less than the effective vertical stress, that is under liquefaction limit as there was no intersection of excess pore pressure curves and effective stress line. Excess pore pressure increased with depth nearly linearly, and the maximum Δu happened at the bottom of the soil model.

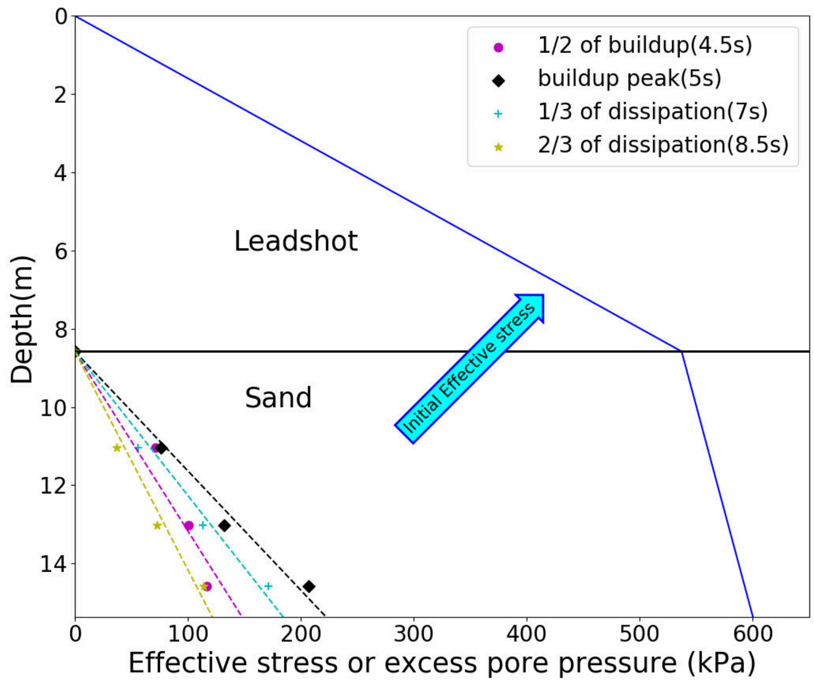

Figure 5. Excess pore water pressure profile. The scattered points and dashed curves represent the excess pore pressure at different times and the corresponding fitting curves. The blue solid line shows the initial vertical effective stress with depth. The solid black horizontal line represents the separation depth of dry lead shot and saturated sand model, or the water level.

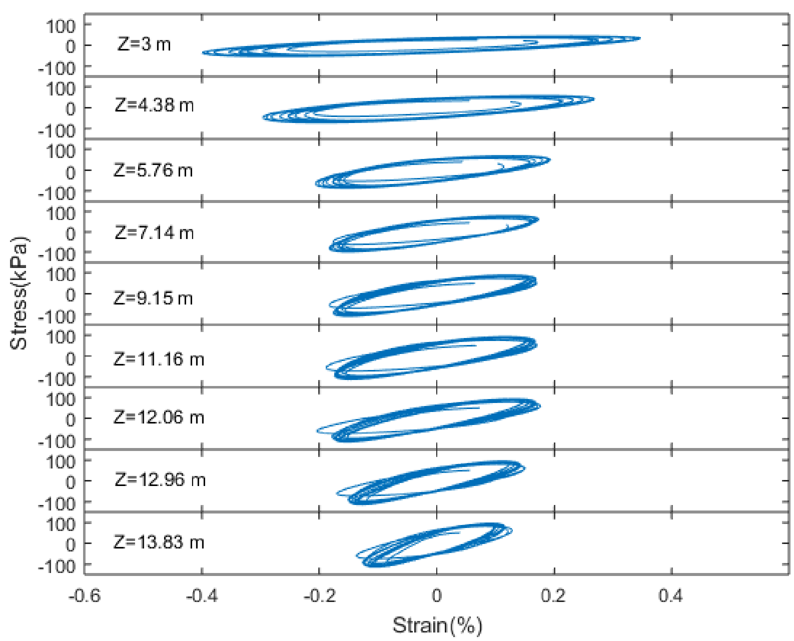

Figure 6. Stress stain loops at nine different depths of shake 2

Stresses and Strains

The stress and strain time histories were calculated using an established System Identification

(SI) technique, developed by Zeghal et al. (1995). SI enables estimating shear stress and strain time histories only from acceleration records at different depths based on a shear beam simulation of the sand model.

Based on the stress and strain time histories calculated with SI technique, the stress strain loops were plotted in Figure 6. The bottom four subfigures correspond to the depths inside the sand model, the top four are in the lead shot layer, and the middle subfigure at depth 9.15m is in the transition layer (a mixture of gravel and coarse sand). As shown in Figure 6, all the nine curves show that the strain was slightly decreasing with depth due to the increased overburden pressure with depth. Considering the comprehensive effects of increased stress and decreased strain with depth, the secant shear modulus in the sand layer was increasing with depth under high effective overburden pressure.

Cyclic strain and Pore Pressure Buildup

Dobry and Abdoun (2015) proposed a plot of maximum pore pressure ratio ($(r_u)_{max}$) versus cyclic shear strain (γ_c) based on the centrifuge and large-scale base shaking tests on uniform saturated sand deposit, conducted by Abdoun et al. (2013). The cyclic shear strain (γ_c) in the graph was determined by System Identification based on acceleration time histories at different depths. Also the test results of this primary shake event are plotted on the graph, shown in Figure 7. In the figure, the value of maximum pore pressure ratio corresponds to the measurement at bottom layer, and the cyclic shear strain values of different shakes are the median γ_c of the middle layer under the overburden pressure of 6atm. The figure indicates that the cyclic shear strain required for pore pressure buildup is larger under higher overburden pressures.

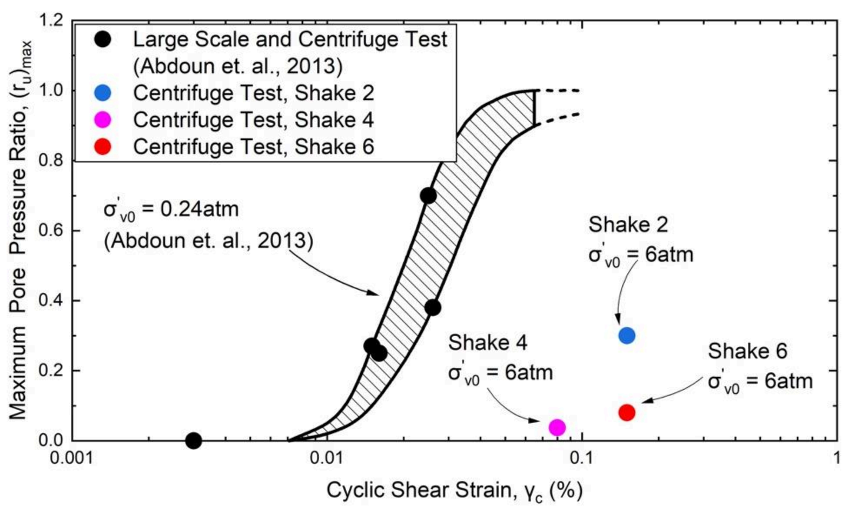

Figure 7. Maximum measured excess pore pressure ratio versus cyclic shear strain (Abdoun et al. 2013, Dobry and Abdoun 2015)

Pre-shaking Effects Under High Confining Pressure

Another two primary shake events were conducted after shake 2. And the effects of pre-shaking were analyzed based on the comparison of the three seismic motions in three aspects: pore pressure build-up, shear wave velocity, and settlement changes.

Pore Pressure Build-up

For all of the destructive shaking events, the maximum excess pore pressure ratio happened at the bottom layer of the sand deposit, and the excess pore pressure buildup around the free surface was close to zero, regardless of the value of the maximum excess pore pressure values were.

None of the three destructive seismic motions liquefied the sand deposit due to the following three reasons: 1) the dry lead shot layer on top of sand deposit provided a free dissipation surface; 2) the high effective overburden pressure of 6atm made it harder to liquefy the sand deposit; 3) the high void ratio of Monterey sand deposit with a Dr = 40% lead to high permeability, thus a high dissipation rate.

The excess pore pressure buildup decreased with pre-shakings, indicating the increased liquefaction resistance due to pre-shakings, as shown in Figure 8. This observation further validated the work performed by El-Sekelly et al. (2015, 2016). In their research, El-Sekelly et al. conducted several centrifuge experiments on clean and silty sand to study the effect of previous preshaking history on the liquefaction resistance of sandy deposit. They found that preshaking events with an excess pore pressure buildup short of liquefaction can gradually increase the soil liquefaction resistance. However, if the deposit is subjected to extensive liquefaction, the liquefaction resistance can dramatically decrease rather than increase.

According to Figure 7, the required cyclic shear strain for excess pore pressure buildup increased with the intensity and number of pre-shaking history by comparing the value of shake 2, 4 and 6.

Settlement Changes

The settlements of centrifuge model measured at the top of the model before and after each seismic motion are summarized in Table 1. According to the settlement values, the model was densified after each destructive motion, but the extent of densification was reduced by pre-shaking history, even with the same shaking amplitude by comparing the settlement values from shake 2 and shake 6. This observation is similar to that observed by El-Sekelly et al. (2015, 2016) in their centrifuge experiments.

Table 1. Settlement records from LVDT for each destructive motion

	Settlement (mm)	Amplitude(g)
shake 2	3.7	0.5
shake 4	0.32	0.2
shake 6	0.8	0.5

Shear Wave Velocity

The shear wave velocity of the centrifuge model was measured at the mid-depth of the Monterey sand deposit under the effective confining pressure of 6atm, as shown in Table 2. According to Table 2, the shear wave velocities increased with intensity and the number of destructive pre-shaking history in the first two shakings, but remained constant after shake 4, not exactly corresponding to the trend of centrifuge model densification. This is consistent with the results reported by El-Sekelly (2014) that deposition method and soil fabric has much more effect on shear wave velocity than densification of the deposit, especially after shaking the deposit for few times.

Table 2. Shear Wave Velocities before and after destructive motions

	Time	V_s (m/sec)	V_{s1} (m/sec)
Initial value		240.28	154.94
shake 2	before	240.28	154.94
	after	254.15	163.88
shake 4	before	254.15	163.88
	after	259.70	167.46
shake 6	before	259.70	167.46
	after	259.70	167.46

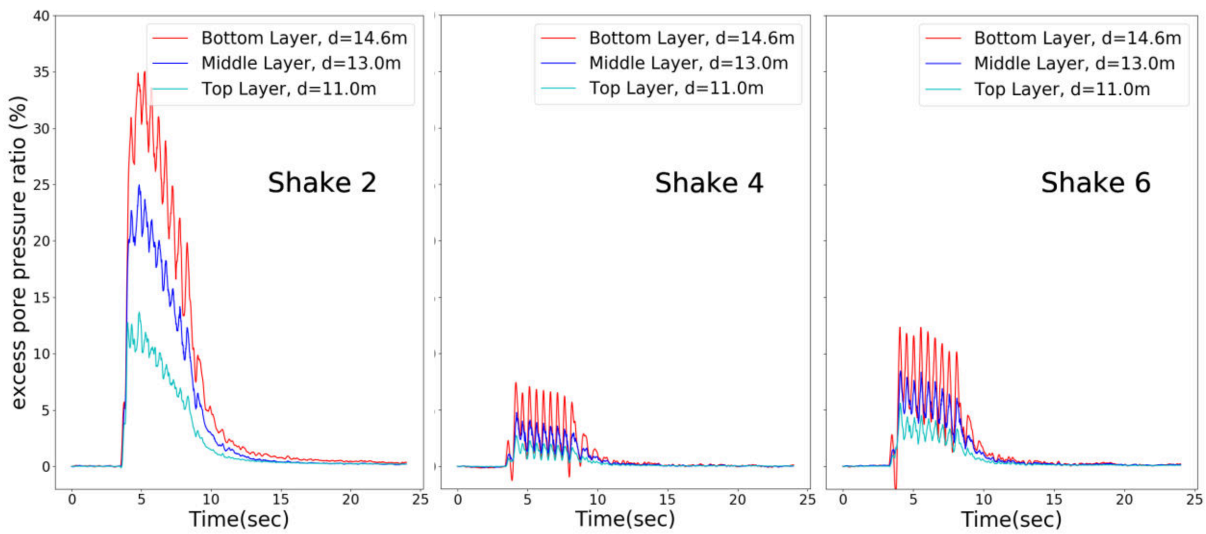

Figure 8. Excess pore pressure ratio during three different destructive seismic motions

CONCLUSION

An innovative technique of building centrifuge model under high a confining pressure was proposed. The outcomes of the new centrifuge model and the effects of pre-shaking history under the high confining pressure were presented. The excess pore pressure buildup and dissipation, shear wave velocities and acceleration time histories were recorded and analyzed. Under high confining pressure, the required cyclic shear strain for a certain excess pore pressure buildup was higher than that of a centrifuge model under the low confining pressure. Furthermore, the required cyclic shear strain also increases with pre-shaking. Normalized shear wave velocities might increase with pre-shaking history, changing from 155 to 167m/sec in shake 2 and 4, but the increasing trend stopped after a certain amount of pre-shakings. The centrifuge model was densified after the destructive shake events, and the densification level was affected by the pre-shaking history. The results also show that, under a high confining pressure, the tendency for reaching full liquefaction decreased due to pre-shaking history.

REFERENCES

Abdoun, T., Gonzalez, M. A., Thevanayagam, S., Dobry, R., Elgamal, A., & Zeghal, M., et al. (2013). “Centrifuge and large-scale modeling of seismic pore pressures in sands: cyclic strain interpretation”. *Journal of Geotechnical & Geoenvironmental Engineering*, 138(8), 1215-1234.

Chen, L., Hou, L., Cao, Z., Yuan, X., Sun, R., Wang, W., ... & Dong, L. (2008). Liquefaction investigation of Wenchuan earthquake. *14th World Conf. on Earthquake Engineering*.

Dobry, R., & Abdoun, T. (2015). Cyclic shear strain needed for liquefaction triggering and assessment of overburden pressure factor K_σ. *Journal of Geotechnical and Geoenvironmental Engineering*, 141(11), 04015047.

El-Sekelly, W., Abdoun, T., and Dobry, R. (2012). Soil characterization in centrifuge models through measurement of shear wave velocities using bender elements. In GeoCongress 2012: State of the Art and Practice in Geotechnical Engineering (pp. 2037-2047).

El-Sekelly, W.(2014). “The Effect of Seismic Preshaking History on the Liquefaction Resistance of Granular Soil Deposits”. *Rensselaer Polytechnic Institute*.

El-Sekelly, W., Tessari, A., and Abdoun, T. (2014). Shear wave velocity measurement in the centrifuge using bender elements. Geotechnical Testing Journal, 37(4), 689-704.

El-Sekelly, W., Abdoun, T., & Dobry, R. (2015). Liquefaction resistance of a silty sand deposit subjected to preshaking followed by extensive liquefaction. *Journal of Geotechnical and Geoenvironmental Engineering*, 142(4), 04015101.

El-Sekelly, W., Dobry, R., Abdoun, T., & Steidl, J. H. (2016). Centrifuge modeling of the effect of preshaking on the liquefaction resistance of silty sand deposits. *Journal of Geotechnical and Geoenvironmental Engineering*, 142(6), 04016012.

Hushmand, B., Scott, R. F., & Crouse, C. B. (1988). “Centrifuge Liquefaction Tests in a Laminar Box”. *Geotechnique*, 38(2), 253-262.

Marcuson III, W. F., & Krinitzsky, E. L. (1976). Dynamic Analysis of Fort Peck Dam (No. WES-TR-S-76-1). *Army Engineer Waterways experiment station Vicksburg Miss*.

Seed, H. B. ‘‘Earthquake-resistant design of earth dams.’’ *Proc., Symp. Seismic Des. Of Earth Dams and Caverns*, ASCE, New York,(1983) 41–64.

Sharp, M. K., Dobry, R., & Abdoun, T. (2003). Liquefaction Centrifuge Modeling of Sands of Different Permeability. *Journal of geotechnical and geoenvironmental engineering*, 129(12), 1083-1091.

Vaid, Y. P., and J. Thomas. (1995). "Liquefaction and postliquefaction behavior of sand." *Journal of Geotechnical Engineering* 121, no. 2: 163-173.

Vaid, Y. P., and S. Sivathayalan. (1996). "Static and cyclic liquefaction potential of Fraser Delta sand in simple shear and triaxial tests." *Canadian Geotechnical Journal* 33, no. 2: 281-289.

Zeghal M, A. W. Elgamal, H. T. Tang, and J. C. Stepp. (1995). “Lotung downhole array. II: evaluation of soil nonlinear properties,”*Journal of Geotechnical Engineering*, vol. 121, no. 4, pp. 363–378.

The Propagation Mechanics of Liquefied Sand Lenses Due to Cyclic Loading

Luis E. Vallejo, Ph.D., M.ASCE[1]; and Vincent Scovazzo, Ph.D.[2]

[1]Professor, Dept. of Civil and Environmental Engineering, Univ. of Pittsburgh, Pittsburgh, PA 15261. E-mail: vallejo@pitt.edu
[2]Project Engineer, John T. Boyd, Canonsburg, PA 15317. E-mail: v-scovaz@jtboyd.com

ABSTRACT

Saturated sand lenses are usually encountered inside saturated clay deposits. During an earthquake the sand lenses could liquefy. After liquefaction, sand volcanoes appear on the surface of the clay deposits. To date, there is not a clear understanding of the mechanisms involved with the movement of the liquefied sand lenses. The liquefaction of the sand lenses is the result of shear stresses induced in the sand by seismic shear (S) waves. Another seismic wave that has been overlooked in the movement of liquefied sand lenses is the compressive (P) wave. This study presents a laboratory experiment that uses a shaking table that vibrates horizontally a saturated clay mass containing a simulated liquefied sand lense. The experiments indicated that the liquefied sand lense moved as a result of the compressive stress induced in the clay by the P waves and the stress concentration at the top of the sand lense.

INTRODUCTION

Sand lenses are frequently encountered in saturated clay deposits located in areas prone to earthquakes (Youd and Hoose, 1976; Amick, et al., 1990) (Fig. 1). Sand lenses are associated with fluvial deposits. They have a semi-elliptical shape and are found to be vertically aligned in the clay deposits as shown in Fig. 1.

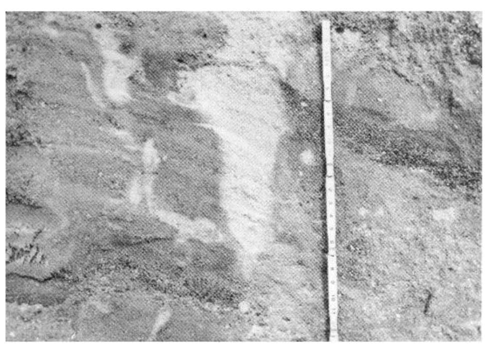

Figure 1. Semi-elliptical sand lense located in a clay deposit in Charleston, S.C. (Amick et al, 1990)

When an earthquake takes place, the sand lenses liquefy. After liquefaction, sand volcanos form on the surface of the clay deposits containing the lenses. To date, there is not a clear explanation of the mechanisms involved in the movement of the liquefied sand lenses from their original location in the clay deposits. The cause of the liquefaction of the sand lenses is assumed to be the shear stresses induced by seismic shear waves (Seed, 1968; Holchin and Vallejo, 1995). Another very important seismic wave that has been overlooked in liquefaction and post-liquefaction studies of sand is the compressive or P wave. The P wave, which is faster than the shear wave, causes the ground to expand and contract in a cyclic manner. If the ground is made of a saturated clay with dispersed liquefied sand lenses, the compressive wave can cause their movement toward the surface of the clay deposit that contains it. The liquefaction is the result of excess pore water pressures induced by shear (S) waves. The movement of the liquefied sand lenses could be the result of compressive (P) waves.

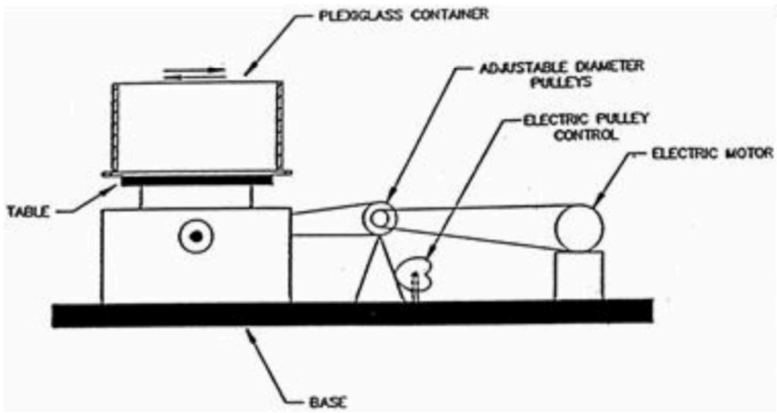

Figure 2. Shaking table apparatus

The purpose of this study is to present the results of a laboratory investigation involving shaking table tests on a saturated clay sample that contains a simulated liquefied sand lense. The clay sample is located inside a box that is horizontally vibrated. The vertical boundary of the box exerts a compressive stress on the clay and liquid sand lense that is simulated using oil. Using this experiment, the mechanism responsible for the movement of the liquid sand from inside the clay and toward its surface was investigated

LABORATORY INVESTIGATION

Shaking Table

The shaking table used in this investigation was a Model No. 10HA built by the All-American Tool & Manufacturing Company (Fig.2). A one half horse power motor vibrated a flat steel plate horizontally for a travel distance of 0.76 cm. A dual adjustable pulley system allowed the vibrations to vary from 5 to 35 Hz.

A Plexiglass container was mounted on the steel plate. The inside dimensions of the container were 30.5 cm in length, 12.7 cm in height, and 10.2 cm in width. The container was constructed with 0.48 cm thick Plexiglass. Inside the container, two rubber foam layers measuring 2.54 cm in thickness, 10.2 cm in width and 30.5 cm in height were attached to the ends of the Plexiglass. The purpose of the foam was to allow lateral movement of the clay mass during the shaking table tests. Fig. 3 shows a general outline of the Plexiglass container with the two rubber foam layers attached to the two extremes of the Plexiglass container. Fig. 3(A) also shows the location of the clay mass that contains an elliptical void filled with oil.

Materials Used in the Experiment

Kaolinite clay was used for the experiments. The clay had a LL = 38%, a PL = 20%, a PI = 18%, and a specific gravity, $G_s = 2.60$. A mixture of clay and water was first slightly consolidated for 5 hours under a pressure of 10 kPa in a rectangular mold. The mold measured 30.5 cm in length, 12.7 cm in height and was 10.2 cm in thickness. After consolidation, the mixture had a water content equal to 56%, a degree of saturation S = 100%, and a unit weight equal to 16.18 kN/m^3. The undrained shear strength of the clay-water mixture was equal to 0.314 kPa. The strength was measured using a vane.

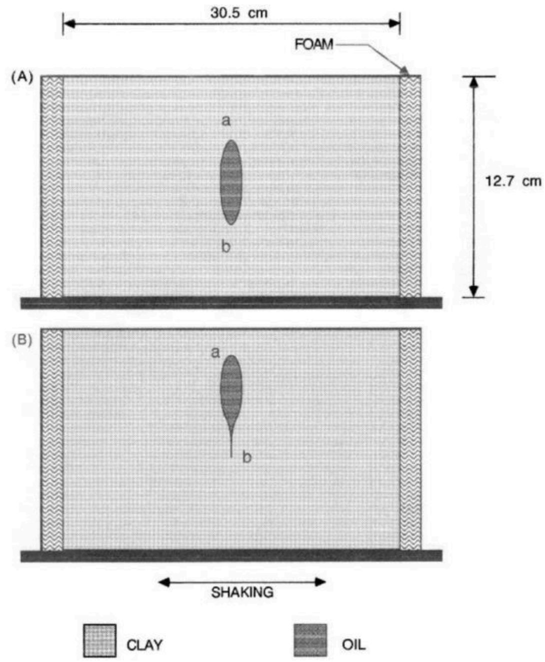

Figure 3 Description of shaking table experiment: (A) before shaking, (B) during shaking

Using a metallic elliptical hollow form with sharp edges, an elliptical void was made in the clay. The elliptical opening covered the total thickness of the clay mass (10.2 cm). The height of the ellipse was 8.3 cm. The center of the ellipse was 2.6 cm wide. The top tip of the void was located 2.8 cm from the top of the clay mass [Fig. 3 (A)]. The clay sample with the elliptical opening was removed from the rectangular mold where it was prepared and then it was placed inside the Plexiglass container. In order to facilitate the insertion of the clay mass into the Plexiglass container, the vertical faces of the container were rubbed with grease

After the clay mass was inside the Plexiglass container, oil inserted with a syringe was used to fill the elliptical void. The small opening made in the clay by the syringe closed and healed properly in a very short time. The viscosity of the oil used was equal to 0.1 Pa-sec. The viscosity of the oil used in the experiments is very similar to that of liquid soil as reported by Middleton and Wilcock (1994). Thus, using oil to simulate liquid sand is warranted. The unit weight of the oil was equal to 8.92 kN/m^3.

Also, a scale analysis conducted by Scovazzo (1999) following the guidelines established by Hubbert (1937), indicated that field conditions were well represented in the experiments using the clay and oil with the engineering properties mentioned above. In addition, the orientation of the elliptical opening in the clay sample (the longest axis vertical), simulates the orientation of an ascending liquefied sand lense in the field (Fig. 1). Also, x-ray analysis conducted by Scovazzo (1999) on the clay sample with the elliptical opening indicated that the process of inserting and removing the elliptical mold with sharp edges did not disturb the boundary region of the elliptical opening in the clay. The boundary region of the elliptical opening was found to remain smooth and undisturbed. The boundary of the elliptical opening kept the fabric of the intact clay forming the rest of the clay sample.